

The effect of small forward speed on prediction of wave loads in restricted water depth

Amitava Guha* and Jeffrey Falzarano

Marine Dynamics Laboratory, Department of Ocean Engineering, Texas A&M University, College Station, Texas, USA 77840-3136

(Received August 19, 2016, Revised October 8, 2016, Accepted October 14, 2016)

Abstract. Wave load prediction at zero forward speed using finite depth Green function is a well-established method regularly used in the offshore and marine industry. The forward speed approximation in deep water condition, although with limitations, is also found to be quite useful for engineering applications. However, analysis of vessels with forward speed in finite water depth still requires efficient computing methods. In this paper, a method for analysis of wave induced forces and corresponding motion on freely floating three-dimensional bodies with low to moderate forward speed is presented. A finite depth Green function is developed and incorporated in a 3D frequency domain potential flow based tool to allow consideration of finite (or shallow) water depth conditions. First order forces and moments and mean second order forces and moments in six degree of freedom are obtained. The effect of hull flare angle in predicting added resistance is incorporated. This implementation provides the unique capability of predicting added resistance in finite water depth with flare angle effect using a Green function approach. The results are validated using a half immersed sphere and S-175 ship. Finally, the effect of finite depth on a tanker with forward speed is presented.

Keywords: green function; shallow water; forward speed; potential theory; added resistance; flare angle

1. Introduction

The recent trend in building ultra large vessels such as the Maersk Triple E class container ship, Prelude FLNG and SHI's 330m long FPSO created renewed interest in understanding the behavior of floating structures with forward speed in deep and restricted water depths. The large draft of these vessels requires consideration of seabed clearance for most harbors and even for operating condition in the open seas. Also, to design channels connecting the harbor to sea, it is important to study the vertical motions of a ship to ensure no grounding occurs during the passage. For this, the prediction of the hydrodynamic coefficient and 6DOF motion of the vessel traveling with a steady forward speed in finite water depth is of interest.

The second order drift forces are also very important for designing mooring systems and side by side offloading operations. Finite depth effects must be considered in the calculation of drift forces and the corresponding effect on vessel motion to ensure the mooring line tension and vessel offsets are within the bounds for safe operation. It was found that the water depth effects on

*Corresponding author, Dr., E-mail: tava.amitava@email.tamu.edu

hydrodynamic coefficients becomes perceptible when the water depth is less than about four times the draft of the ship, defined here as intermediate water depth. When the depth to draft ratio becomes less than 2, the effect of the bottom becomes significant and is considered to be shallow water.

The close proximity of the seabed affects the vessel motion in two ways. First, the incident waves change due to a restricted water depth where the wavelength is related to depth by the dispersion relation. Secondly, the hydrodynamic coefficients such as the added mass, radiation damping and diffraction forces changes due to the bottom boundary condition. These hydrodynamic coefficients can be obtained using potential theory by applying the finite depth Green function.

In this paper, the development of a new finite depth Green function is explained which is then implemented in an existing 3D panel method program named MDLHydroD (Guha 2012, Guha and Falzarano 2015, 2016, 2013). The forward speed approximations are applied using encounter frequency and simplified m-terms. The results obtained show a significant effect of forward speed and water depth on wave excitation forces and vessel motion.

2. Formulation

The boundary value problem is formulated with a body (floating or fully submerged) traveling with steady forward speed U or equivalently fixed in a current of equal magnitude and opposite direction. Regular waves of incidence frequency ω_I with heading angle β and amplitude A , traveling in uniform water depth h are considered. The relation between finite water depth and the wave frequency is expressed as the dispersion relation $\omega^2 = kg \tanh(kh)$, where k is the wave number. To solve the dispersion relation an efficient code applying higher order iterative technique following (Newman 1990) is developed.

The forward speed changes the frequency at which the body encounters the waves, which is expressed as the encounter frequency $\omega_e = \omega_I - k_I U \cos \beta$. The unsteady fluid potential around the body is given by

$$\Phi(\vec{x}, t) = [-Ux + \phi_S(\vec{x})] + \left[\phi_I(\vec{x}, \beta, \omega_I) + \phi_D(\vec{x}, \beta, \omega_I) + \sum_{j=1}^6 \eta_j \phi_j(\vec{x}, U, \omega_e) \right] e^{i\omega_e t} \quad (1)$$

where ϕ_S is the steady disturbance potential due to forward motion of the body in calm water. ϕ_I is the potential due to incident wave, ϕ_D is the diffraction potential and ϕ_j is the radiation potential. η_j is the motion amplitude of the body in 6 degrees of freedom. The continuity condition in the fluid domain gives the Laplace equation

$$\nabla^2 \Phi = 0 \quad (2)$$

where the potential can be solved by applying the following boundary conditions:

1. Combined dynamic and kinematic free surface boundary condition: $\left[\left(i\omega_e - U \frac{\partial}{\partial x} \right)^2 + g \frac{\partial}{\partial z} \right] (\phi_I, \phi_D, \phi_j) = 0$ on $z = 0$
2. The bottom boundary condition: $\frac{\partial}{\partial z} (\phi_I, \phi_D, \phi_j) = 0$ on $z = -h$

3. The Sommerfeld radiation condition: $\lim_{kr \rightarrow \infty} \sqrt{kr} \left(\frac{\partial}{\partial r} - ik \right) (\phi - \phi_I) = 0$
4. The body surface no-penetration boundary condition:
 - a. Radiation: $\frac{\partial \phi_j}{\partial n} = i\omega_e n_j + Um_j$ on S
 - b. Diffraction: $\frac{\partial \phi_I}{\partial n} + \frac{\partial \phi_D}{\partial n} = 0$ on S

where simplified $m_j \approx (0,0,0,0, n_3, -n_2)$ terms with body normal $\vec{n} = (n_1, n_2, n_3)$ are applied. The linear incident wave potential satisfying above boundary conditions is given by

$$\phi_I = \frac{igA \cosh(k_I(z+h))}{\omega_I \cosh(k_I h)} e^{-ik_I(x \cos \beta + y \sin \beta)} \tag{3}$$

An approximation to the radiation potential for low to moderate forward speed can be obtained using the zero speed potential as

$$\begin{aligned} \phi_j &= \phi_j^0 \text{ for } j = 1,2,3,4 \\ \phi_5 &= \phi_5^0 + \frac{U}{i\omega_e} \phi_3^0 \\ \phi_6 &= \phi_6^0 - \frac{U}{i\omega_e} \phi_2^0 \end{aligned} \tag{4}$$

Analytical solutions for the radiation potential ϕ_j and the diffraction potential ϕ_D are generally not available for arbitrary shaped bodies, which necessitates the use of numerical techniques such as the source distribution method.

2.1 The source distribution method

To obtain the diffraction and radiation velocity potentials, the body surface is discretized into N quadrilateral panels of area ΔS_j and a source of unknown strength is distributed uniformly over each panel. The zero speed velocity potential can be written in terms of the unknown source strength σ as

$$\phi^0 = \frac{1}{4\pi} \int_S \sigma(\vec{x}_s) G(\vec{x}, \vec{x}_s) ds \tag{5}$$

where \vec{x} is the field point where the potential is being evaluated due to a source at \vec{x}_s . Here, $G(\vec{x}, \vec{x}_s)$ is the finite depth Green function which satisfies the free surface, bottom and radiation boundary conditions. Applying the body boundary condition gives

$$-\frac{1}{2}\sigma_i + \frac{1}{4\pi} \sum_{j=1}^N \sigma(\vec{x}_s) \frac{\partial G}{\partial n}(\vec{x}, \vec{x}_s) \Delta S_j = \begin{cases} i\omega_e n_j : \text{Radiation} \\ -\frac{\partial \phi_I}{\partial n} : \text{Diffraction} \end{cases} \tag{6}$$

This system of linear equations is solved using efficient matrix inversion algorithms to obtain the source strength σ_i on each panel.

2.2 The finite depth green function

In obtaining the source strength on each panel of the body, the most computationally burdensome aspect is due to the Green function evaluation. For a body with N panels, the Green function must be evaluated for at least $(N - 1) \times (N - 1)$ times and 4 times more in the case of a higher order integration method such as Gauss quadrature, which consumes a large portion of the CPU time. To overcome this, an efficient finite depth Green function has been developed. The analytical form of the finite depth Green function is given in (John 1949, 1950) which is also summarized in (Wehausen & Laitone, 1960). In terms of numerical stability and the computational efficiency the finite depth Green function is divided into two separate functions which are used in the domain $\frac{R}{h} < 0.5$ and $R/h \geq 0.5$, where $R = [(x - \xi)^2 + (y - \eta)^2]^{1/2}$ is the horizontal distance from the source $q(\xi, \eta, \zeta)$ to the field point $p(x, y, z)$.

2.3 Integral form of the green function

The integral form of the Green function is suitable for $\frac{R}{h} < 0.5$ and found to be unstable for $\frac{R}{h} > 7$. The analytical form of this function is given by (Wehausen and Laitone 1960) as

$$G(p; q) = \frac{1}{r} + \frac{1}{r^*} + 2PV \int_0^\infty \frac{(\mu + K)e^{-\mu h} \cosh(\mu(\zeta + h)) \cosh(\mu(z + h))}{\mu \sinh(\mu h) - K \cosh(\mu h)} J_0(\mu R) d\mu + i \frac{2\pi(k + K)e^{-kh} \sinh(kh) \cosh(k(\zeta + h)) \cosh(k(z + h))}{Kh + \sinh^2(kh)} J_0(kR) \quad (7)$$

where PV represents the principal value integral and

$$K = \frac{\omega^2}{g} = k \tanh(kh)$$

$$r = [(x - \xi)^2 + (y - \eta)^2 + (z - \zeta)^2]^{1/2}$$

$$r^* = [(x - \xi)^2 + (y - \eta)^2 + (z + 2h + \zeta)^2]^{1/2}$$

$$R = [(x - \xi)^2 + (y - \eta)^2]^{1/2} \quad (8)$$

The solution of the Rankine part for both source and the image source is obtained using the method described by (Hess and Smith 1964). The full numerical implementation details for this is given in (Guha 2012). The imaginary part of the Green function can be directly calculated. The numerical difficulty is presented mostly by the principal value integral part of the Green function. Using the method of substitution the singularity of the function is removed and a form that can be numerically integrated is obtained. The Gauss-Laguerre quadrature is implemented to efficiently obtain the value of the integral.

2.4 Series form of the green function

The series form of the Green function is applicable for the rest of the domain $\frac{R}{h} \geq 0.5$. (John

1949, 1950) derived the infinite series expansion for the finite depth Green function as

$$G(p; q) = 2\pi \frac{K^2 - k^2}{k^2h - K^2h + K} \cosh(k(z + h)) \cosh(k(\zeta + h)) [Y_0(kR) + iJ_0(kR)] + 4 \sum_{n=1}^{\infty} \frac{k_n^2 + K^2}{k_n^2h + K^2h - K} \cos(k_n(z + h)) \cos(k_n(\zeta + h)) K(k_nR) \tag{9}$$

where k_n denotes the set of corresponding positive real roots of equation: $k_n \tanh(k_n h) = -K$. Again, the function can be broken into real and imaginary parts. The imaginary part can be rewritten using the relation given by (Wehausen and Laitone 1960) to be equal to the imaginary part of the integral form of the Green function which can be calculated directly. The real part of the Green function has a singularity at $\frac{R}{h} = 0$ and takes a significantly large number of terms in the infinite sum to give a converged solution. However, for the domain $\frac{R}{h} \geq 0.5$ a six decimal accuracy can be achieved by using approximately $6h/R$ number of terms. To be consistent, the algorithm is developed to iterate until a 7 significant digit accuracy is achieved.

A number of comparisons are made with published data to establish the accuracy and validity of the code. Fig. 1 shows for the case $Kh = 5$ the comparison between the series and integral Green function with that of (Li 2001) and (Monacella 1966). Further validations can be found in (Guha 2016).

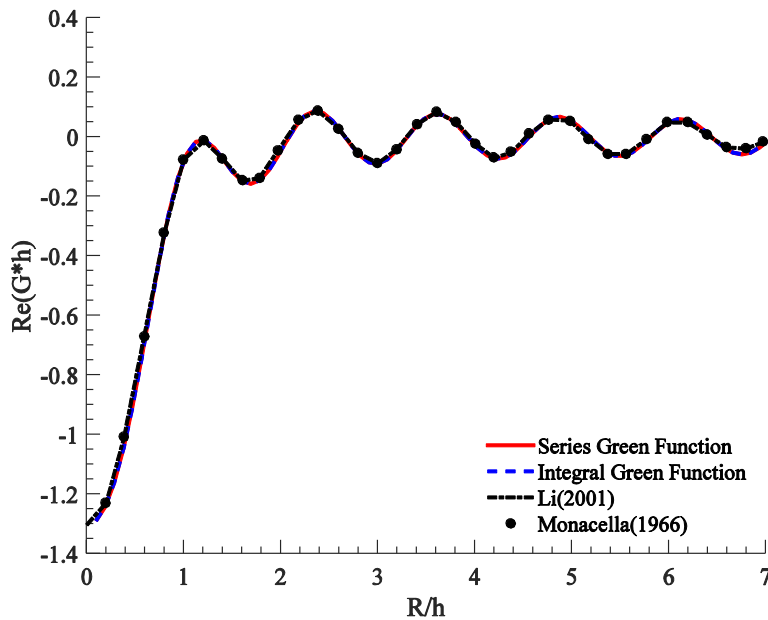


Fig. 1 The real part of Gh when $Kh = 5.0$, $kh = 5.000454$ and $0 < R/h < 7$

2.5 Forces and motions of the body

The forces and moments on the body are obtained by integrating the pressure over the submerged body surface. The pressure is obtained from the velocity potential by applying the Bernoulli's equation

$$P = \frac{1}{2}\rho U^2 - \rho \frac{\partial \Phi}{\partial t} - \frac{1}{2}\rho |\nabla \Phi|^2 - \rho g z \quad (10)$$

The hydrodynamic force can be obtained by

$$F_{Hj} = - \int_S P n_j ds \quad j = 1, 2, \dots, 6 \quad (11)$$

The added mass and damping is obtained by integrating the radiation pressure over the hull as

$$A_{jk}^0 = - \frac{\rho}{\omega_e} \int_S \text{Im}(\phi_k) n_j ds \quad B_{jk}^0 = - \rho \int_S \text{Re}(\phi_k) n_j ds \quad (12)$$

followed by forward speed corrections as described in (Guha and Falzarano 2016). The wave excitation force due to incident wave also known as the Froude-Krylov force is obtained as

$$F_I = i \omega_I \rho \int_S \phi_I n_j ds \quad (13)$$

and the force due to diffracted wave is

$$\begin{aligned} F_D &= \rho \int_S (i \omega_e n_j - U m_j) \phi_D ds \\ &= - \rho \int_S \phi_j^0 \frac{\partial \phi_I}{\partial n} ds \quad \text{for } j = 1, 2, 3, 4 \\ &= - \rho \int_S \phi_j^0 \frac{\partial \phi_I}{\partial n} ds + \frac{\rho U}{i \omega_e} \int_S \phi_3^0 \frac{\partial \phi_I}{\partial n} ds \quad \text{for } j = 5 \\ &= - \rho \int_S \phi_j^0 \frac{\partial \phi_I}{\partial n} ds - \frac{\rho U}{i \omega_e} \int_S \phi_2^0 \frac{\partial \phi_I}{\partial n} ds \quad \text{for } j = 6 \end{aligned} \quad (14)$$

The calculated added mass, damping and wave excitation forces are used to solve the equation of motion to get the vessel response as

$$\sum_{k=1}^6 [-\omega_e^2 (M_{jk} + A_{jk}) + i \omega_e B_{jk} + C_{jk}] \eta_k = F_j^I + F_j^D \quad \text{for } j = 1, 2, \dots, 6 \quad (15)$$

where M_{jk} is the mass matrix, C_{jk} is the hydrostatic stiffness matrix and η_k the vessel response in k^{th} mode of motion.

2.6 Calculation of the second order mean drift forces

The influence of second order mean drift forces are proven to be of critical importance in the prediction of stability criteria for floating bodies as well in determining the integrity of the mooring system design. Numerical prediction of the mean drift forces rely primarily upon two

methods. First, the far field method proposed by (Maruo 1960) which is based on diffracted and radiated wave energy and the momentum flux at infinity. Second is the near field method first proposed by (Boese 1970) and later modified by (Pinkster 1979) and (Faltinsen, Minsaas *et al.* 1980). This method is more intuitive and gives forces in all 6DOF compared to the former which can only provide forces in 3DOF. In the near field method, a perturbation approach is applied to differentiate zeroth, first and second order quantities and the forces and moments are simply obtained by integrating the hydrodynamic pressure on the body surface.

The velocity potential ϕ , wave elevation ζ relative wave elevation ζ_r , body motion amplitude η and the pressure p are perturbed using a small parameter ϵ of the order of the wave slope assuming small amplitude oscillation of the body about a mean position.

$$\begin{aligned}\phi &= \epsilon\phi^{(1)} + \epsilon^2\phi^{(2)} + \dots \\ \zeta &= \epsilon\zeta^{(1)} + \epsilon^2\zeta^{(2)} + \dots \\ \zeta_r &= \epsilon\zeta_r^{(1)} + \epsilon^2\zeta_r^{(2)} + \dots \\ \vec{\eta}_r &= \epsilon\vec{\eta}^{(1)} + \epsilon^2\vec{\eta}^{(2)} + \dots \\ p &= p^{(0)} + \epsilon p^{(1)} + \epsilon^2 p^{(2)} + \dots\end{aligned}\tag{16}$$

Substituting the above expressions into the Bernoulli's Eq. (10) gives the expression for zeroth, first and second order pressures. Similarly, the perturbation of the hydrodynamic force in Eq. (11) give

$$\vec{F} = -\left(\int_{S_0} ds + \int_{wl} \zeta_r dl\right) (p^{(0)} + \epsilon p^{(1)} + \epsilon^2 p^{(2)}) (\vec{n}^{(0)} + \epsilon(\vec{\theta}^{(1)} \times \vec{n}^{(0)}) + \epsilon^2 H \vec{n}^{(0)})\tag{17}$$

Separating terms with ϵ^2 gives the second order force equation as

$$\begin{aligned}\vec{F}^{(2)} &= -\int_{wl} \frac{1}{2} \rho g (\zeta_r^{(1)})^2 \frac{\vec{n}^{(0)}}{\sqrt{1-n_3^2}} dl \\ &+ \int_{S_0} \rho \left(\frac{\partial\phi^{(2)}}{\partial t} - U \frac{\partial\phi^{(2)}}{\partial x}\right) \vec{n}^{(0)} ds \\ &+ \int_{S_0} \frac{\rho}{2} \left\{ \left(\frac{\partial\phi^{(1)}}{\partial x}\right)^2 + \left(\frac{\partial\phi^{(1)}}{\partial y}\right)^2 + \left(\frac{\partial\phi^{(1)}}{\partial z}\right)^2 \right\} \vec{n}^{(0)} ds \\ &+ \int_{S_0} i\omega_e \rho \left\{ (\eta_1 - \eta_6 y_B + \eta_5 z_B) \frac{\partial\phi^{(1)}}{\partial x} + (\eta_2 + \eta_6 x_B - \eta_4 z_B) \frac{\partial\phi^{(1)}}{\partial y} \right. \\ &+ \left. (\eta_3 + \eta_5 x_B - \eta_4 y_B) \frac{\partial\phi^{(1)}}{\partial z} \right\} \vec{n}^{(0)} ds \\ &- \rho g A^{(0)} \left[\eta_4 \eta_6 x_{B,f} + \eta_5 \eta_6 y_{B,f} + \frac{1}{2} (\eta_4^2 + \eta_5^2) Z_0 \right] \hat{k} \\ &- \omega_e^2 \{ -\eta_2 \eta_6 m + \eta_4 \eta_6 m z_g - \eta_6 \eta_6 m x_g + \eta_3 \eta_5 m + \eta_4 \eta_5 y_g - \eta_5 \eta_5 m x_g \} \hat{i} \\ &- \omega_e^2 \{ \eta_1 \eta_6 m + \eta_5 \eta_6 m z_g - \eta_6 \eta_6 m y_g - \eta_3 \eta_4 m - \eta_4 \eta_4 m y_g + \eta_4 \eta_5 m x_g \} \hat{j} \\ &- \omega_e^2 \{ -\eta_1 \eta_6 m - \eta_5 \eta_5 m z_g + \eta_5 \eta_6 m y_g + \eta_2 \eta_4 m - \eta_4 \eta_4 m z_g + \eta_4 \eta_6 m x_g \} \hat{k}\end{aligned}\tag{18}$$

Taking a time average over one wave period cancels the term with the second order potential and the rest of the terms can be evaluated from the linear potential theory. Similarly the second order moment terms can be obtained, but excluded from here for brevity (See (Guha 2016)). These forces are known as the mean drift forces. A critical term included here is the multiplication of $\frac{\bar{n}^{(0)}}{\sqrt{1-n_3^2}}$ with the waterline integral term, which allows consideration of hull emergence angle (or flare angle) in prediction of added resistance. This is found to be of significant importance as shown in (Guha and Falzarano 2015).

It must be noted that the zero speed Green function is used in the forward speed calculations using the approximations suggested by (Salvesen, Tuck *et al.* 1970) and (McTaggart 2002) which limits the applicability of the code to low to moderate forward speed.

3. Results and discussion

3.1 Validation of finite depth hydrodynamic load predictions at zero forward speed

The finite depth hydrodynamic results are compared with an industry standard program (Lee 2013). The container ship S175 as shown in Fig. 2 is used for validating the first order motions and second order forces. The heave and pitch motion RAOs are compared in Figs. 3 and 4. The heave and pitch drift forces are compared in Figs. 5 and 6. The calculated results were found to be in good agreement with the industry standard code.

A truncated floating cylinder of radius $R = 1$ m and draft $T = 0.5$ m (Fig. 7) is also considered to validate the developed code at three different water depths with depth to draft ratio $h/T = 2, 4$ and 8. Fig. 8 shows the comparison results with the commercial code for all three depths.

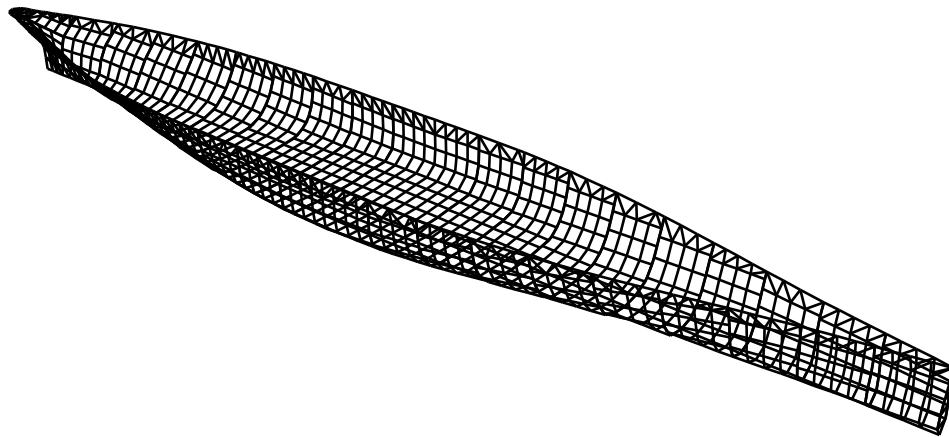


Fig. 2 Panel model of the S175 container ship with 1202 number of panels

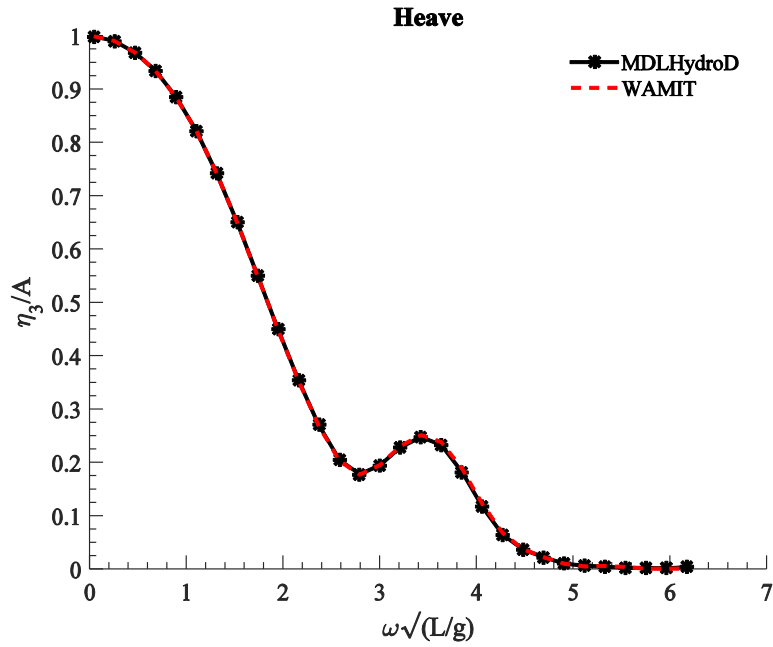


Fig. 3 Comparison of heave RAO for S175 container ship for water depth to draft $\frac{d}{T} = 2$

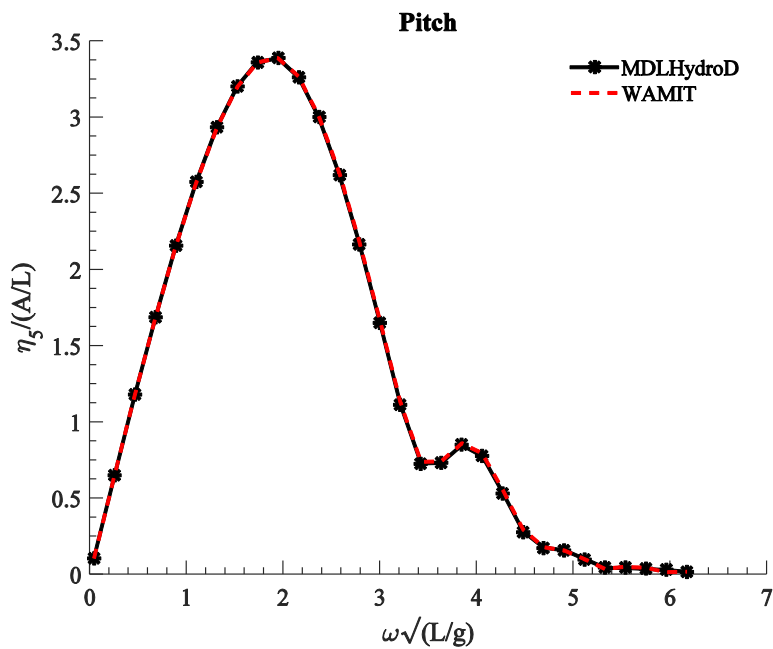


Fig. 4 Comparison of pitch RAO for S175 container ship for water depth to draft $\frac{d}{T} = 2$

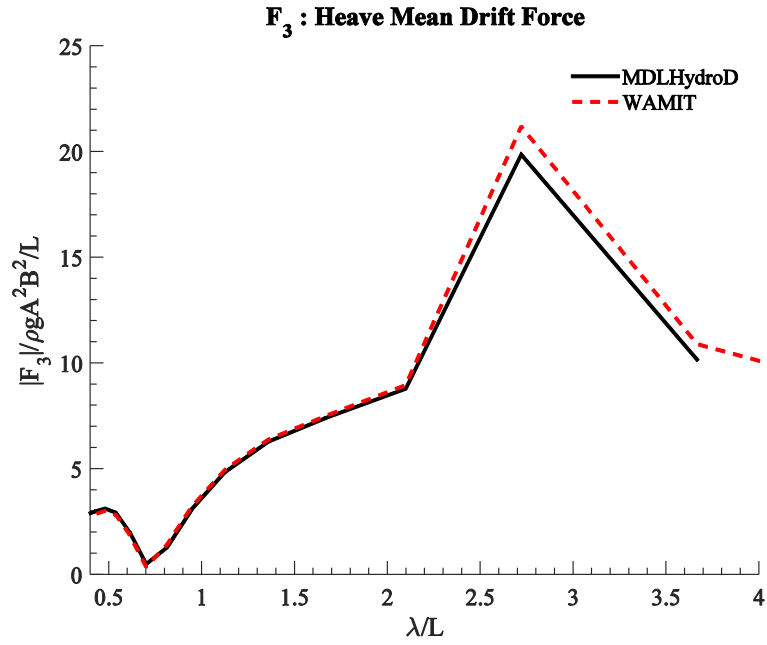


Fig. 5 Comparison of heave drift force for S175 container ship for water depth to draft ratio $\frac{d}{T} = 2$

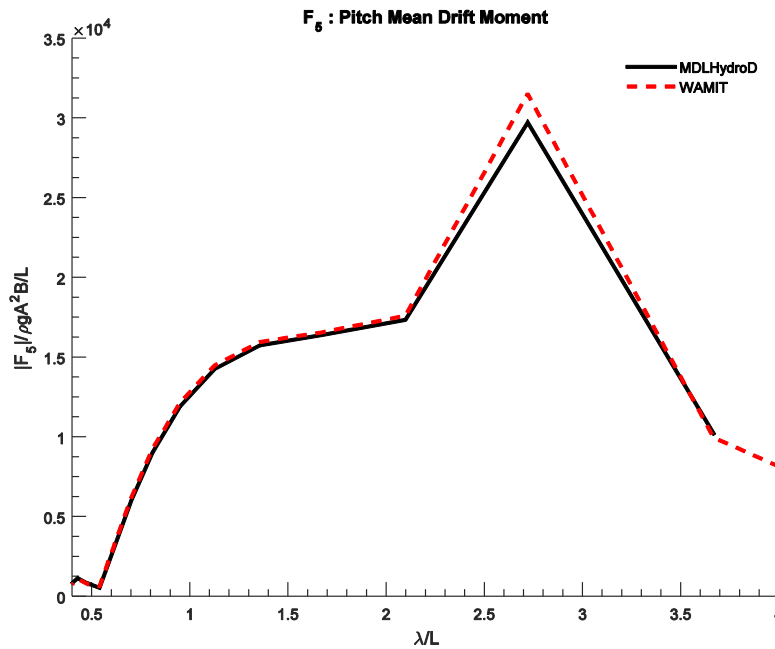


Fig. 6 Comparison of pitch drift force for S175 container ship for water depth to draft ratio $\frac{d}{T} = 2$

It can be observed that the results from both codes are essentially identical. The other phenomena that can be observed from these results is that the heave motion RAO at $h/T = 2$ is significantly different than the $h/T = 4$ and $h/T = 8$ showing the effect of the shallow water depth. Also, the effect of water depth on hydrodynamic coefficients becomes insignificant beyond the $h/T = 4$ and the deep water Green function can be used for these cases. It should be noted here that the deep water Green function is significantly faster (about 1000 times) compared to the finite depth Green function.

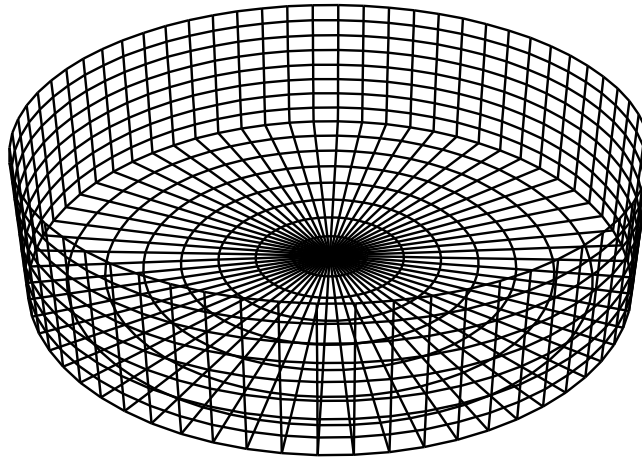


Fig. 7 Panel model of the floating cylinder of $R = 1\text{ m}$, $T = 0.5\text{ m}$ with 1024 panels

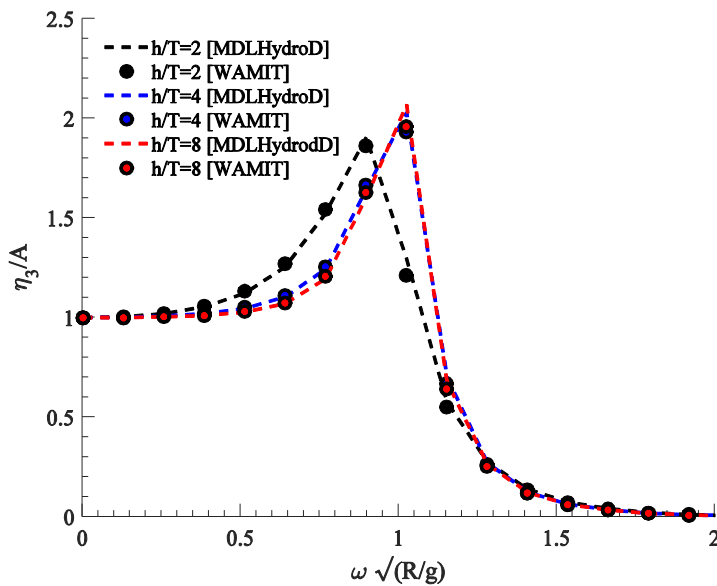


Fig. 8 Comparison of a floating cylinder of $R=1\text{ m}$, $T=0.5\text{ m}$ for water depth to draft ratio $h/T = 2,4,8$

3.2 Validation of finite depth hydrodynamic load predictions at low forward speed

The forward speed analysis at finite water depth is significantly more complicated compared to the deep water. A number of parameters begin to change with reduction in the water depth which needs to be considered while performing such analysis. In terms of the floating body dimension, two factors may be defined to investigate the effect of the water depth. First, the ratio between the wave length and water depth which is characterized by kh where k is the wave number. Second, the ratio of the water depth to the body draft (h/T) which signifies the seabed clearance. Along with this, there is the forward speed effect which is represented by Froude number $Fn = U/\sqrt{gL}$, where L is the characteristic length of the body.

The experimental or computational results are very limited for the forward speed finite depth condition. Here, the results obtained by (Grue and Biberg 1993) for a floating hemisphere (Fig. 9) translating at a low forward speed at various water depth is compared.

Fig. 10 shows the comparison of surge force and Fig. 11 shows the comparison of heave force at $h/R = \infty$ and $h/R = 1.2$ compared with those of (Grue and Biberg 1993). Both cases the results were found to be in excellent agreement with the published results.

3.3 Effect of water depth on vessel motion and added resistance

To understand the effect of water depth on motion and added resistance, a tanker hull is chosen. The principal particulars of the hull is given in Table 1. The deep water or infinite water depth condition is plotted in black colored lines. The red and blue lines represent water depth corresponding to $h/T = 3$ and $h/T = 1.5$ respectively. The heave and pitch motion and the added resistance are calculated for three forward speeds corresponding to $Fn = 0, 0.13$ and 0.26 in head sea condition.

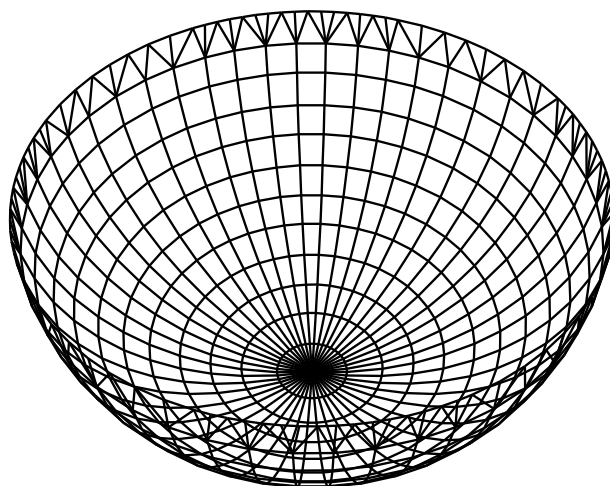


Fig. 9 Panel model of the floating hemisphere of radius 10 m with 672 number of panels

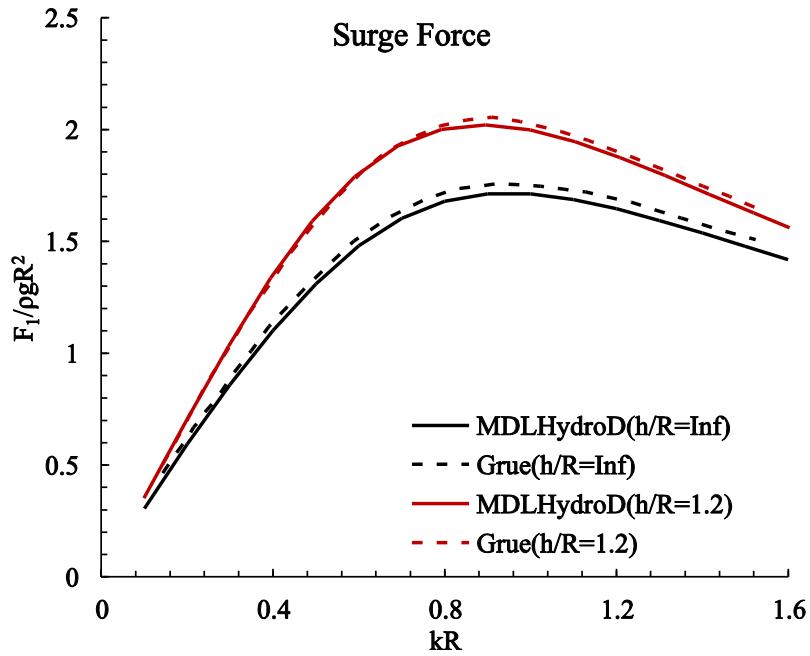


Fig. 10 Surge force comparison for floating hemisphere of radius 10 m at $Fn = 0.04$ in deep and shallow water depths

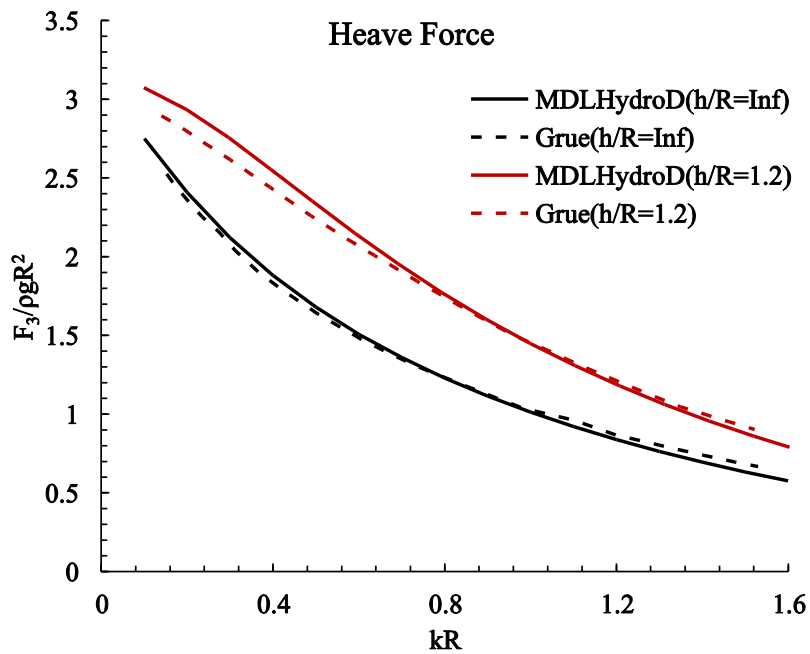


Fig. 11 Heave force comparison for floating hemisphere of radius 10 m at $Fn = 0.04$ in deep and shallow water depths

Figs. 12-14 show the results for the zero speed case where it can be observed that the water depth has almost no effect on the vessel motion or the drift forces. Where Fig. 15 to Fig. 20 shows that with an increase of forward speed the effect of water depth becomes more perceptible. Both motion and added resistance were found to be reduced with a decrease in water depth. While this may be the favorable condition when a ship enters the port channel, the viscous effects of the seabed are expected to be more significant which is not considered in the potential flow method applied here. One should also consider the squat and trim of the vessel in shallow water to avoid vessel grounding. This method however provides a quick way to evaluate the vertical motions expected for ships entering intermediate water depths or analysis of platforms operating in finite water depths.

Table 1 Principal particulars of the Tanker

Length	L	158.5	m
Breadth	B	23.2	m
Draft	T	7.75	m
Displacement	Δ	18000	t
Longitudinal Center of Gravity	LCG	0.317	m
Radius of Gyration in Roll	k_{xx}	49.927	m
Radius of Gyration in Pitch	k_{yy}	39.625	m
Radius of Gyration in Yaw	k_{zz}	39.625	m

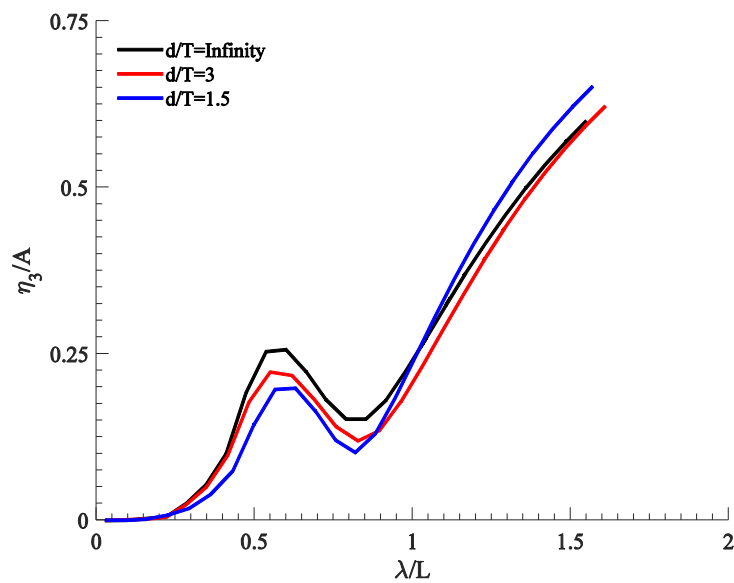


Fig. 12 Heave amplitude at $F_n = 0$ in head sea condition

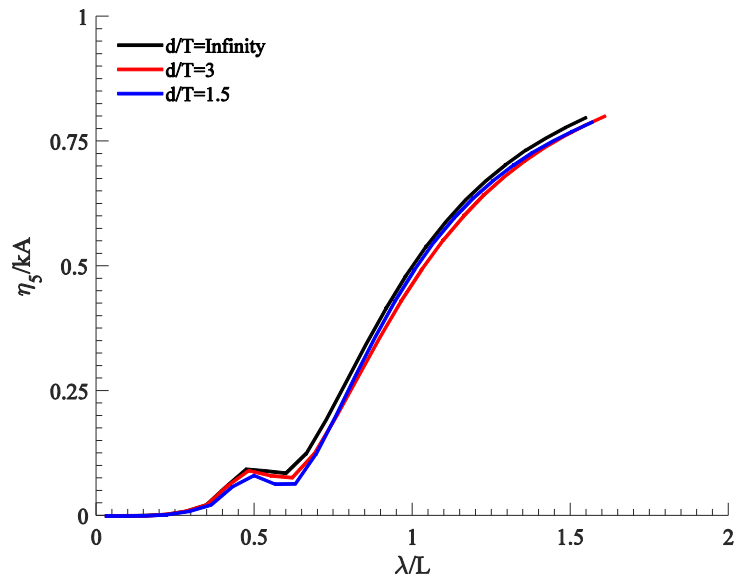


Fig. 13 Pitch amplitude at $Fn = 0$ in head sea condition

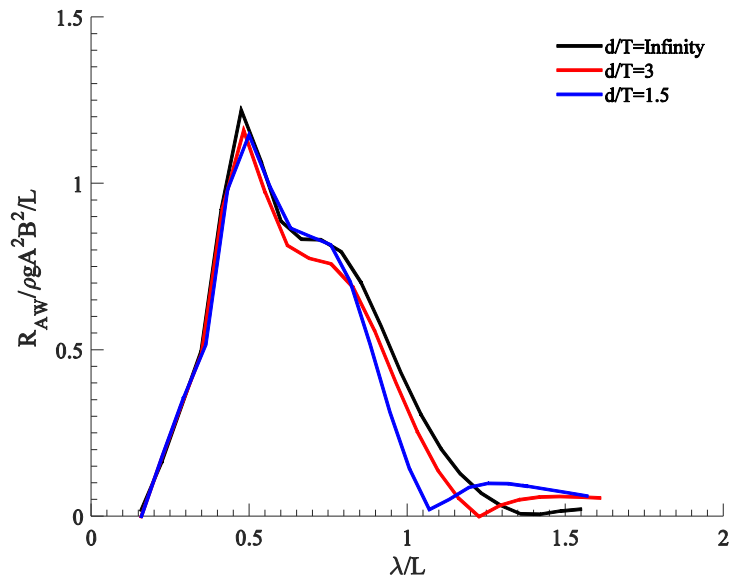
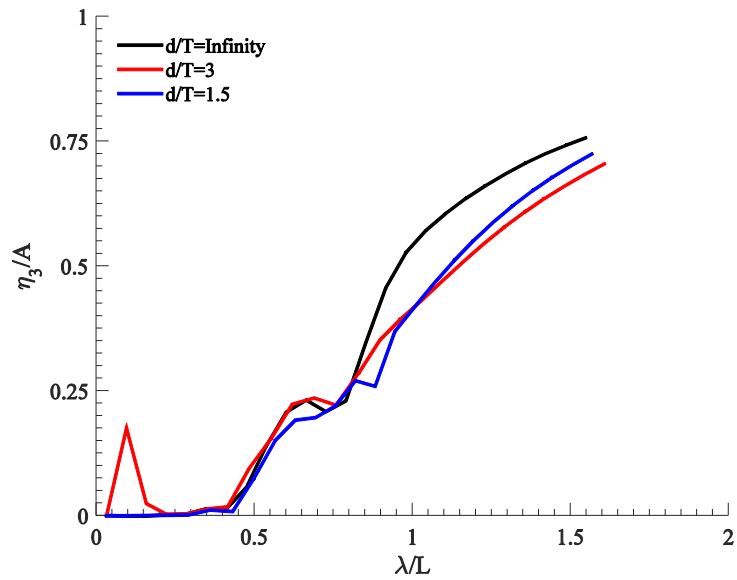
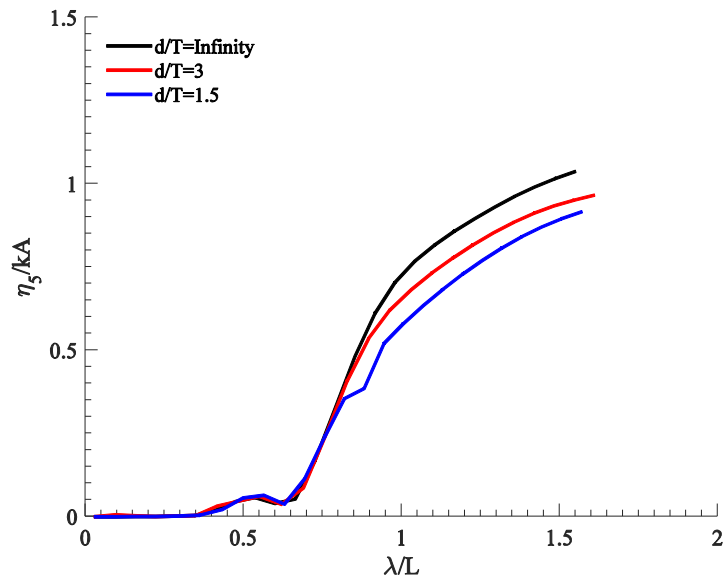


Fig. 14 Surge mean drift force at $Fn = 0$ in head sea condition

Fig. 15 Heave amplitude at $Fn = 0.13$ in head sea conditionFig. 16 Pitch amplitude at $Fn = 0.13$ in head sea condition

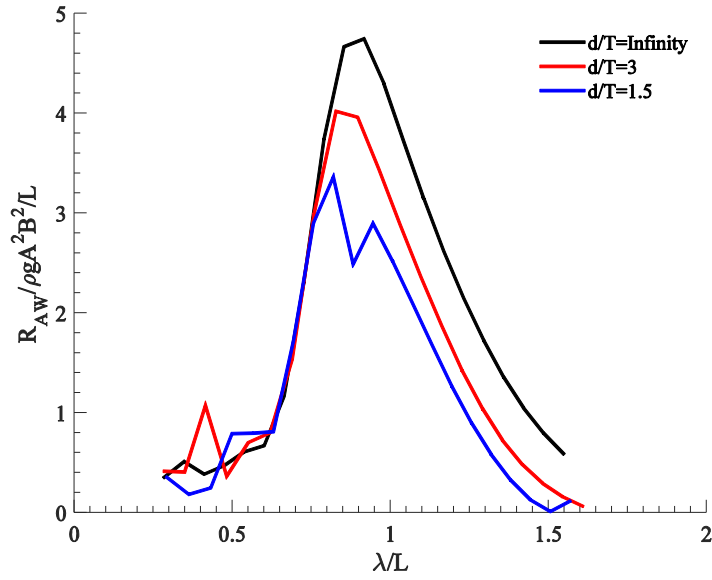


Fig. 17 Added resistance at $Fn = 0.13$ in head sea condition

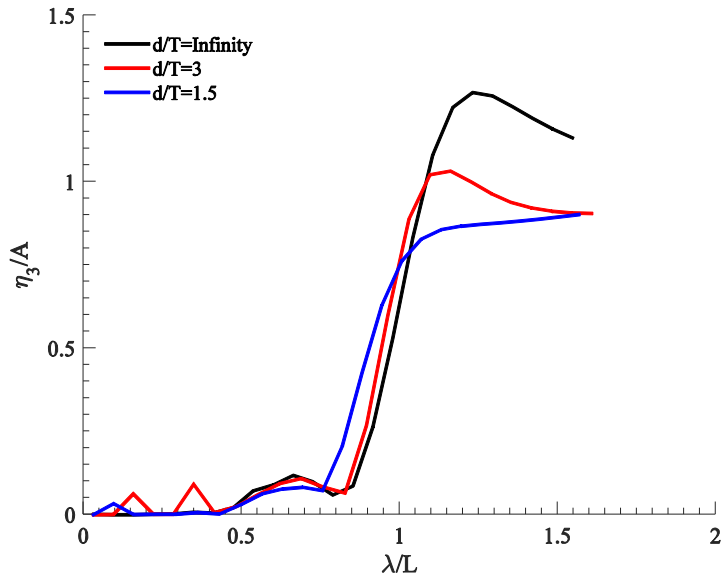


Fig. 18 Heave amplitude at $Fn = 0.26$ in head sea condition

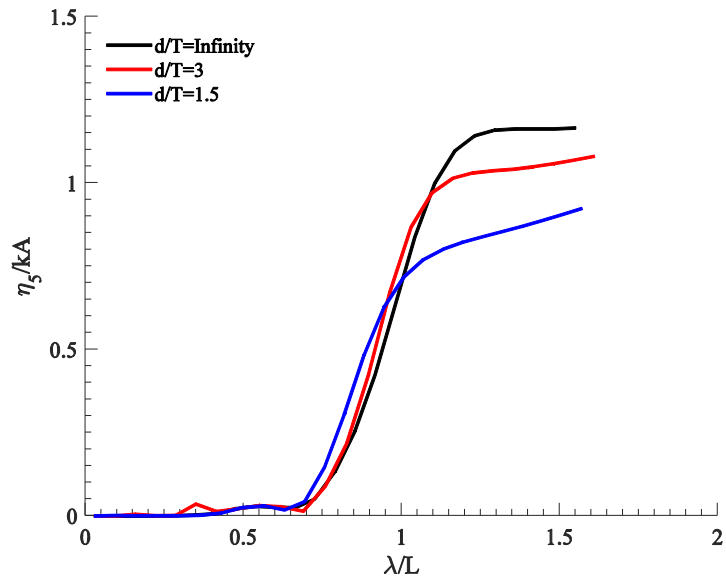


Fig. 19 Pitch amplitude at $Fn = 0.26$ in head sea condition

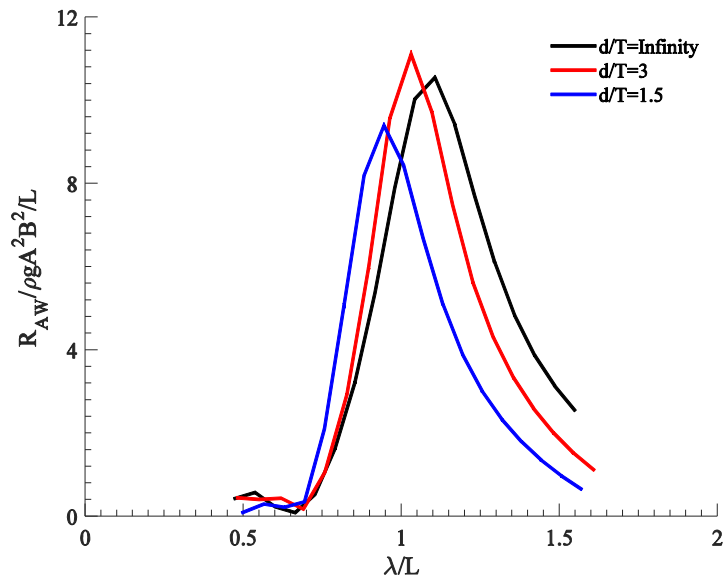


Fig. 20 Added resistance at $Fn = 0.26$ in head sea condition

4. Conclusions

This paper presents a potential theory application in predicting wave induced loads and motions of floating bodies with low to moderate forward speed in finite water depth. A Green function approach is followed, as it allows performing the hydrodynamic analysis using only discretized underwater hull surface. A new finite depth Green function is developed for this purpose and implemented in an existing panel method code capable of considering forward speed effects. The results were validated using industry standard tools for finite depth zero speed conditions for the S175 container ship and published results for finite depth forward speed condition for a floating hemisphere. A tanker hull is then analyzed to show the effect of forward speed and water depth on vessel motion and drift forces. Further validation for higher forward speed in finite depth needs to be performed to establish applicability of the developed code for real applications.

Acknowledgements

The continuation of hydrodynamic tool development work was supported in part by the Office of Naval Research (ONR Grant N00014-16-1-2281). The authors would like to thank Dr. Paul Hess and Andy Silver (NSWC-Carderock) for supporting this work. The authors also acknowledge the help of Alex Landsburg for the partial funding provided by Society of Naval Architects and Marine Engineers (SNAME) to support this work.

References

- Boese, P. (1970), "Eine einfache methode zur berechnung der widerstandserhöhung eines schiffes im seegang", *J. Schiffstechnik*, **17**(86), 1-18.
- Faltinsen, O., Minsaas, K., Liapis, N. and Skjørdaal, S. (1980), "Prediction of resistance and propulsion of a ship in a seaway", *Proceedings of the 13th Symposium on Naval Hydrodynamics*, Tokyo, Japan.
- Grue, J. and Biberg, D. (1993), "Wave forces on marine structures with small speed in water of restricted depth", *App. Ocean Res.*, **15**(3), 121-135. [http://doi.org/10.1016/0141-1187\(93\)90036-W](http://doi.org/10.1016/0141-1187(93)90036-W)
- Guha, A. (2012), *Development of a computer program for three dimensional frequency domain analysis of zero speed first order wave body interaction* (Thesis). Texas A&M University, College Station, TX.
- Guha, A. (2016), *Development and application of a potential flow computer program: Determining first and second order wave forces at zero and forward speed in deep and intermediate water depth*. Texas A&M University, College Station, TX.
- Guha, A. and Falzarano, J. (2015), "The effect of hull emergence angle on the near field formulation of added resistance", *Ocean Eng.*, **105**(1), 10-24. <http://doi.org/10.1016/j.oceaneng.2015.06.012>
- Guha, A. and Falzarano, J. (2016), "Estimation of hydrodynamic forces and motion of ships with steady forward speed", *Int. Shipbuild. Prog.*, **62**(3-4), 113-138. <http://doi.org/10.3233/ISP-150118>
- Guha, A. and Falzarano, J.M. (2013), "Development of a computer program for three dimensional analysis of zero speed first order wave body interaction in frequency domain", *Proceedings of the ASME 2013 32nd International Conference on Ocean, Offshore and Arctic Engineering*, Nantes, France. <http://doi.org/10.1115/OMAE2013-11601>
- Hess, J.L. and Smith, A.M. (1964), "Calculation of non-lifting potential flow about arbitrary three-dimensional bodies", *J. Ship Res.*, **8**(3), 22-44.
- John, F. (1949), "On the motion of floating bodies I", *Commun. Pure Appl. Math.*, **2**(1), 13-57.
- John, F. (1950), "On the motion of floating bodies II. Simple harmonic motions", *Commun. Pure Appl.*

- Math.*, **3**(1), 45-101.
- Lee, C.H. (2013), *WAMIT User Manual*. Chestnut Hill, MA, USA.
- Li, L. (2001), *Numerical seakeeping predictions of shallow water effect on two ship interactions in waves*. Dalhousie University.
- Maruo, H. (1960), Wave resistance of a ship in regular head seas, *Bulletin of the Faculty of Engineering, Yokohama National University*, 9(March).
- McTaggart, K.A. (2002), *Three dimensional ship hydrodynamic coefficients using the zero forward speed Green function* (Report) (Vol. 59), Defence Research Development Canada, Ottawa.
- Monacella, V.J. (1966), "The disturbance due to a slender ship oscillating in waves in a fluid of finite depth", *J. Ship Res.*, **10**(4), 242-252.
- Newman, J. (1990), "Numerical solutions of the water-wave dispersion relation", *Appl. Ocean Res.*, 12(1), 14-18. [http://doi.org/10.1016/S0141-1187\(05\)80013-6](http://doi.org/10.1016/S0141-1187(05)80013-6)
- Pinkster, J.A. (1979), "Mean and low frequency wave drifting forces on floating structures", *Ocean Eng.*, **6**(1), 593-615.
- Salvesen, N., Tuck, E.O. and Faltinsen, O.M. (1970). "Ship motions and sea loads", *T. Soc. Naval Archit. Marine Engineers*, **78**, 250-287.
- Wehausen, J.V. and Laitone, E.V. (1960), "Surface waves", *Encyclopedia Phys.*, **9**, 446-815.

MK